Journal of Solid State Chemistry 184 (2011) 1428–1432

Contents lists available at ScienceDirect

Journal of Solid State Chemistry

journal homepage: www.elsevier.com/locate/jssc

Heavy doping of H^- ion in $12CaO \cdot 7Al_2O_3$

Katsuro Hayashi *

Center for Secure Materials, Materials and Structures Laboratory, Tokyo Institute of Technology, R3-34, 4295 Nagatsuta, Yokohama 226-8503, Japan

ARTICLE INFO

Article history:
Received 14 December 2010
Received in revised form
18 February 2011
Accepted 4 April 2011
Available online 12 April 2011

Keywords:
Calcium aluminates
Hydrogen
NMR spectroscopy
Point defects
Electrical conductivity

ABSTRACT

$12CaO \cdot 7Al_2O_3$ (C12A7, mayenite), which has a nanoscale porous structure that can accommodate extraframework species such as hydride (H^-), oxide (O^{2-}), hydroxide (OH^-) ions, and electrons, has been doped with H^- ions to investigate its effects as dominant extraframework species. Chemical doping with CaH_2 enables the concentration of H^- ions to reach almost the theoretical maximum. The concentration of H^- ions is characterized by optical absorption intensity ascribed to photoionization of H^- ions, and ^1H magic angle spinning nuclear magnetic resonance (MAS-NMR) spectroscopy. Persistent electron generation, which is accompanied by the formation of an F^+ absorption band and electrical conductivity, by irradiation with ultraviolet light at room temperature increases as the H^- ion doping increases until it reaches half the theoretical maximum and then decreases as the H^- ion concentration increases further. This dependence indicates that both H^- and O^{2-} ions are necessary for the generation of persistent electrons.

1. Introduction

Over the past several 10 years, H^- ions doped into anion sites of binary alkali halides, which are termed *U*-centers [1,2], and binary alkaline-earth oxides [3,4], have been investigated extensively. These wide-gap transparent hosts provide a suitable environment to investigate the physical properties of H^- ions in solids. Although there are numerous crystal structures and chemical compositions of oxides, only several material systems have been investigated for H^- ion doping [5–14] beyond the binary alkaline-earth oxides. It is still debated whether H^- ion doping into oxide hosts is generally possible or not. Theoretical calculations suggest that when the Fermi level in a material exceeds the 'hydrogen neutrality level', which is rather common in a wide range of materials, the equilibrated charge of hydrogen occupying a certain site favors the negative state (H^-) over the positive one (H^+) [15–17]. Thus, materials that have a shallow conduction band minimum are generally advantageous for the formation of H^- ions, suggesting that many candidate material systems exist. To examine experimentally how general the incorporation of H^- ions into oxides is, it is important to establish control over H^- ion doping, and to be able to detect and quantify it. As a first step, it is convenient to start with the oxide host that has the highest affinity for H^- ions. In this study, the oxide host $12CaO \cdot 7Al_2O_3$ (C12A7, mayenite) is used.

C12A7 is a complex oxide of Ca and Al with a ratio of 12:14, whose stoichiometric (or undoped) unit cell is expressed as $[Ca_{24}Al_{28}O_{64}]^{4+} \cdot 2O^{2-}$. The former part is a positively charged cubic lattice framework possessing a cage structure with an inner free space with a diameter of ~0.4 nm. The latter two O^{2-} ions randomly occupy two of the twelve cages in the unit cell to compensate for the positive charges (Fig. 1). The O^{2-} ions can be exchanged for other various anions, such as OH^- [18–21], F^- [22,23], Cl^- [22], O^- [24,25], O_2^- [24,25], and S^{2-} [26] ions as well as H^- ions [11–14]. In addition, electrons [27–32] can occupy the empty space inside each cage in a similar manner to monovalent anions. So far, full exchange up to the theoretical maximum (total negative charge density of 2.3×10^{21} q cm^{-3}) has been achieved using several extraframework anions [18–23,25] and electrons [28], while the highest concentration of H^- ions has been limited to ~1/10–100 (10^{19-20} cm^{-3}) of the theoretical maximum [11–14]. However, these concentrations, which were obtained simply by annealing in hydrogen gas at less than 1 atm, are much higher than the typical concentration of H^- ions reported in alkali halides, suggesting an excellent affinity of H^- ions for this material.

This high affinity is further substantiated by the thermodynamic assessment described in Ref. [33]. Formation of the 'hydride' of C12A7 (at around 500–700 °C) is described as

$$2e^-(c) + H_2(g) \rightarrow 2H^-(c) \quad \Delta H_{f,\ C12A7:e^-} = -4.5\ eV, \tag{1}$$

where 'c' and 'g' denote the species in a cage and gas phase, respectively. The change of enthalpy for Eq. (1) is lower than that in the corresponding binary reaction:

$$Ca + H_2(g) \rightarrow CaH_2 \quad \Delta H_{f,Ca} = -2.0\ eV, \tag{2}$$

which is the lowest among the formation of binary metal hydrides, that is, CaH_2 is the most stable binary metal hydride.

* Fax: +81 45 924 5365.
E-mail address: k-hayashi@lucid.msl.titech.ac.jp

0022-4596/$ - see front matter © 2011 Elsevier Inc. All rights reserved.
doi:10.1016/j.jssc.2011.04.008

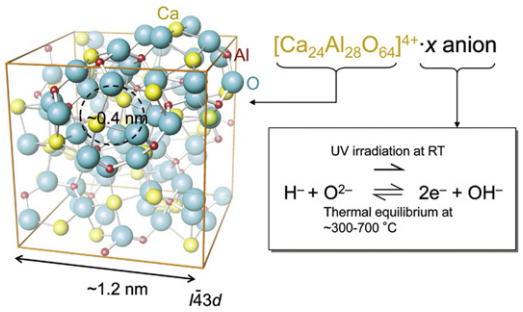

Fig. 1. Lattice framework of C12A7 (unit cell) and species in its cages relevant to electron photogeneration.

If one tries to form hydrides using a hydrogen gas reduction process, the difference in enthalpy changes becomes much larger:

$$O^{2-}(c)+2H_2(g)\rightarrow 2H^-(c)+H_2O(g) \quad \Delta H_{f,C12A7:O2^-}=-3.8\ \text{eV}, \quad (3)$$

$$CaO+2H_2(g)\rightarrow CaH_2+H_2O(g) \quad \Delta H_{f,CaO}=+2.0\ \text{eV}. \quad (4)$$

Thus, the cage site of C12A7 thermodynamically provides one of the best environments for the formation of H^- ions.

The incorporation of electrons into the cages of C12A7 affords C12A7 with electronic conductivity, accompanied by coloration because of the appearance of two optical absorption bands at ~2.8 eV (F^+ band) and ~0.4 eV (polaron band) [34,35]. When the electron concentration, N_{e^-}, is below $\sim 1\times 10^{19}\ cm^{-3}$, each electron is well localized in a cage similar to an F^+ center in alkaline-earth oxides, and inter-cage migration is mediated by thermally activated hopping. As the value of N_{e^-} increases above $5-7\times 10^{20}\ cm^{-3}$, the conductivity mechanism shifts from hopping to metallic conduction [28,32]. So far, two types of electron dopings have been examined. One is direct chemical doping, which has been achieved by thermal reduction treatment with reactive metals [27–32]. The other process is chemical H^- ion doping, followed by illumination with ultraviolet (UV) light [11–14]. We have proposed the following process for persistent electron generation. Photoionization splits an H^- ion into an electron and an atomic hydrogen (H^0) [13]. The transient H^0 thermally releases another electron, and the remaining H^+ ion diffuses until it combines with an O^{2-} ion in another cage to form an OH^- ion. Thus, a pair of H^- and O^{2-} ions acts as a source of two electrons. The overall process can be described as [14]

$$H^-(c)+O^{2-}(c)+null(c)\rightarrow 2e^-(c)+OH^-(c) \quad \Delta H_{2e^-}=+1.4\ \text{eV}, \quad (5)$$

where the *null* indicates empty cage. The reaction in Eq. (5) has been validated by the reasonable agreement between the changes in enthalpy evaluated experimentally from the thermally activated electrical conductivity of H^- ion-doped C12A7 at ~300–700 °C and by a first principle calculation [14,36,37]. The amphoteric changes in valence and high diffusivity at room temperature, which are properties unique to hydrogen, are responsible for reaction in Eq. (5). These properties may be important for designing new materials functions using H^- ion doping in oxides.

The main purpose of this study is to achieve H^- ion doping with the highest possible concentration. We employed a CaH_2 reduction process, which has been used for H^- ion substitution or reduction of certain oxide ion sites in metal oxide hosts [9,10,38,39]. This process enables us to obtain a wide range of H^- ion concentrations, almost up to the theoretical maximum. Furthermore, Eq. (5) is validated from the dependence of the photogenerated electron concentration on the H^- ion concentration.

2. Experimental

Transparent C12A7 crystals refined by the floating zone method were sliced into pieces with a thickness of 0.5 mm, a width of 5 mm and a height of ~5–7 mm. The crystals were doped with H^- ions by annealing using the conditions shown in Table 1.

Samples 1 and 2 were annealed at 1300 °C under a 0.2 atm H_2 atmosphere (N_2 balance) in an alumina tube for 6 h using an electronic furnace, followed by quenching to room temperature. These two samples were exposed to the same annealing conditions, but possessed different concentrations of extraframework anions after annealing. This is empirically ascribed to an unintentional leakage in the electronic furnace. Incorporation of O_2 impurities in an atmosphere enhances the formation of O^{2-} and OH^- ions and suppresses H^- ions and electrons in cages.

Prior to H^- ion doping by annealing, samples 3, 7, and 9–11 were pretreated by fabrication process of 'C12A7 electride' as described in Ref. [27]. In brief, C12A7 slices were heated with metallic Ca shots in an evacuated silica glass tube at 800 °C for 240 h, followed by removal of the reacted layer on the sample surface by mechanical grinding. The chemical composition of C12A7 electride is described as approximately $[e^-]=2$ and $[O^{2-}]=1$ [23] ($N_{e^-}=\sim 1\times 10^{21}\ cm^{-3}$), where the brackets indicate the number of species per unit cell. Sample 3 was annealed with H_2 gas in sealed silica glass capsule. Samples 4–11 were annealed with reducing agents containing hydrogen (CaH_2 powder: 99% purity; Ca shots: 99%; $Ca(OH)_2$ powder: 99.9%; all supplied by Wako Chemicals, Japan) in silica glass capsules at 800 °C. Although many combinations of hydrogen sources, amounts, and annealing times were examined in samples 3–10, the reproducibility of each condition is poor and no clear systematic dependence on the annealing conditions were found for the amount of extraframework species introduced (as examined in Section 3). For example, in two samples (nos. 6 and 8) treated with same process except the annealing time for the reaction with CaH_2, a longer annealing time does not necessarily enhance the incorporation of H^- ion. The reproducibility was improved when a piece of C12A7 crystal and CaH_2 powder were wrapped in Pt foil with a thickness of 50 μm and sealed in an evacuated silica glass capsule (sample 11). This improvement is ascribed to the surrounding CaH_2 powder blocking penetration of oxygen species that are released from or permeate through the silica glass capsule. In addition, direct contact of samples with CaH_2 powder probably enhances the interdiffusion of hydrogen species.

The reactive layer on the surface of all of the annealed samples was removed by mechanical grinding and then polished to a mirror finish. The final thickness of samples ranged from 60 to 200 μm. All absorption spectra were measured using a Hitachi

Table 1
Sample preparation conditions.

Sample	Starting material	Atmosphere/ agent	Annealing condition	Amount of H^- ions [H^-]
1	As grown	0.2 atm H_2 gas	1300 °C for 6 h, quench	0.11(3)
2	As grown	0.2 atm H_2 gas	1300 °C for 6 h, quench	0.26(6)
3	Electride	0.5 atm H_2 gas	800 °C for 40 h	0.28(6)
4	As grown	Ca and CaH_2	800 °C for 40 h	0.34(7)
5	As grown	Ca and $Ca(OH)_2$	800 °C for 80 h	1.0(3)
6	As grown	CaH_2	800 °C for 240 h	1.5(4)
7	Electride	CaH_2	800 °C for 80 h	2.0(5)
8	As grown	CaH_2	800 °C for 40 h	2.2(5)
9	Electride	CaH_2	800 °C for 240 h	2.6(6)
10	Electride	CaH_2	800 °C for 120 h	4(1)
11	Electride	CaH_2	800 °C for 240 h[a]	4(1)

[a] A C12A7 crystal and CaH_2 powder were wrapped with a Pt foil.

U-4000 spectrophotometer before and after illumination with UV light, which was carried out at room temperature using a Xenon lamp until a salutation in the formation of F^+ band.

To calibrate the absolute H^- ion concentration, ^1H magic angle spinning nuclear magnetic resonance (^1H-MAS-NMR) spectra were measured for samples 6 and 11. As a reference sample, a fully OH^- ion-incorporated C12A7 powder with a composition of $[Ca_{24}Al_{28}O_{64}]^{4+}\cdot 4OH^-$ was prepared by annealing C12A7 powder at 900 °C under a wet N_2 atmosphere with a water vapor pressure of 0.02 atm [18]. The measurements were performed on a Bruker Biospin DSX-400 spectrometer operating at a resonance frequency of 400.13 MHz equipped with a high-speed magic angle spinning probe with a diameter of 2.5 mm. Each granulated sample was weighed ($\sim 50-70$ mg) to obtain a quantitative result and sealed in a zirconia rotor. The rotation frequency used was 30 kHz. Spectra were acquired with 90° pulses with a length of 2.5 μs. The measured frequency range was 24 kHz and 215 data points were assigned in the relevant spectrum. A trace of distilled water (+4.65 ppm from tetramethylsilane, TMS) was used as an external secondary reference.

The electrical conductivity of samples 2, 4, and 10 was measured over the temperature range of $\sim 10-300$ K using a cryostat. To avoid a high contact resistance between the electrodes and sample surface, which is caused by surface degradation and the low work function of electron-doped C12A7 [29], impedance spectroscopy was used to evaluate the bulk conductivity.

3. Results

Fig. 2 shows absorption spectra of selected samples in the as-prepared state and after irradiation with UV light at room temperature. The high energy absorption edge of each sample varies significantly. The tail of the absorption edge coincides with the most sensitive energy range (~ 4.0 eV) [11] of UV light-induced electron generation, suggesting that the absorption edge is dominated by the absorption due to H^- ions. Other possible extraframework anions are OH^- and O^{2-} ions. The absorption edges of these species have been well investigated [23]. The absorption coefficient at 4.0 eV is 20 cm^{-1} for the stoichiometric composition ($[O^{2-}]=2$), and is reduced to ~ 0 cm^{-1} for the sample fully exchanged with OH^- ions ($[OH^-]=4$). Accordingly, the absorption edge of all of the samples shows a dominant contribution from H^- ions except for sample 1, where a weak H^- ion absorption band is superimposed onto the tail of an O^{2-} ion absorption band. Overall, the absorption coefficient at 4.0 eV is a good measure for characterizing the amount of H^- ions in a sample. The samples in Table 1 and Fig. 2 are sorted by the absorbance at 4.0 eV, i.e., the amount of H^- ions. First-principle calculations based on an embedded two-cage cluster model predicts the photoexcitation energy of the H^- ion to be 4.3 eV [36,37]. Although the maximum of the H^- band was not observed experimentally because of the high energy of its absorbance, the energy of the absorption tail agrees reasonably with the theoretical prediction. Thus, this absorption band is ascribed to the photoionization of H^- ions.

^1H-MAS-NMR spectra of samples 6 and 11 exhibited a strong signal at chemical shift (δ) of +5.3 ppm with respect to the TMS reference (Fig. 3). Its signal intensity correlates reasonably with the absorption coefficient at 4.0 eV, providing evidence that the NMR signal at +5.3 ppm and the absorption edge can be assigned to H^- ions. The reference sample fully incorporated with OH^- ions ($[OH^-]=4$) exhibited a strong signal at −0.8 ppm. A weak signal at this chemical shift is also detected for sample 6, suggesting that formation of H^- ion was incomplete and a small amount of OH^- ions still remained in this sample. The amount of H^- ions in sample 11 is judged to be nearly the theoretical maximum of $[H^-]=4$ through comparison of the intensity of the peak at +5.3 ppm with that at −0.8 ppm in the reference sample. A reasonable estimation of the H^- ion concentration may be $1.7-2.3\times 10^{21}$ cm^{-3} by taking account of the residual electrons (2×10^{19} cm^{-3}) and photogenerated electrons (2×10^{18} cm^{-3}), the measurement errors ($\sim 20-40\%$) and the spectrum manipulation processes. The lattice constant of sample 11 at 298 K was 11.974(1) Å, which is nearly same as fully OH^- ion-incorporated C12A7 [11.97338(3) Å] and smaller than that of fully O^{2-} ion-incorporated one [11.98748(3) Å] [21]. Theoretical density of C12A7 containing H^-, OH^-, and/or O^{2-} ions as extraframework species are calculated to be ranging from 2.655 to 2.718 g cm^{-3} at 298 K. In the present study, all concentrations of the extraframework species are calculated with assuming a value of 2.69 g cm^{-3}, which causes an additional error of $\sim \pm 1\%$ in the calculations.

Two absorption bands at ~ 0.4 and ~ 2.8 eV (see Fig. 2) arise from inter-cage charge transfer and *s*–*p*-like inter- or intra-cage transitions of electrons in cages, respectively [34,35]. If the electron concentration is less than $\sim 1\times 10^{20}$ cm^{-3}, it can be readily measured from the intensity of either the 2.8 or 0.4 eV bands because of their linear relationship with electron concentration [27]. Because the intensities of both bands are strong, the absorption coefficient at 2.2 eV, which is the tail region of the two bands, was used to evaluate the electron concentration. In sample 1, UV irradiation generates electrons with a concentration of 5×10^{18} cm^{-3}. The concentration of photogenerated electrons is higher in sample 4, which has been more heavily doped than sample 1. In sample 7, the photogenerated electron concentration is so high ($>2\times 10^{20}$ cm^{-3}) that the absorption spectrum was

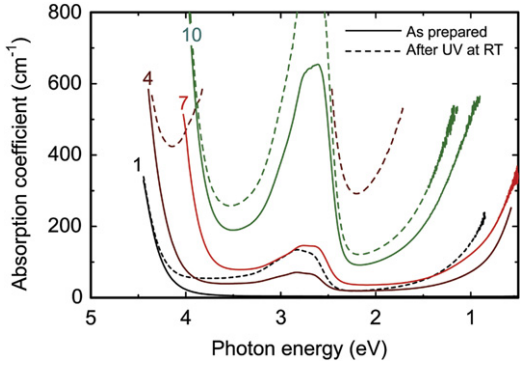

Fig. 2. Optical absorption spectra measured for samples 1, 4, 7, and 10 before (solid lines) and after (dashed lines) UV irradiation. The absorbance of sample 7 after UV irradiation is out of the measurable range.

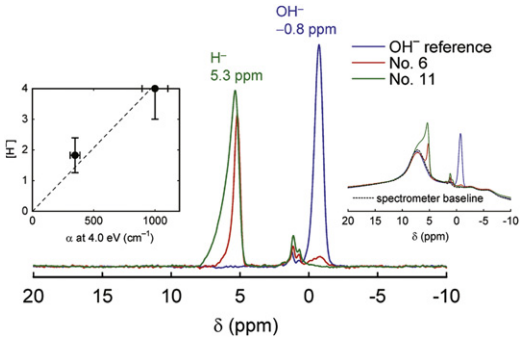

Fig. 3. ^1H-MAS-NMR spectra measured for samples 6 and 11 after background subtraction and normalization by the sample weight. The raw spectra showing the background data are presented in the right inset. Weak signals at 1.2 and 0.7 ppm are caused by contaminants in the spectrometer or rotor. The left inset shows the correlation of the areal intensity of the +5.3 ppm signal and the absorbance at 4.0 eV.

too intense to measure. However, in the most heavily doped sample (no. 10), the concentration of photogenerated electrons is smaller than that in sample 7.

The relationship between the intensity of the optical absorption of H^- ions and the concentration of photogenerated electrons is shown in Fig. 4. The upper horizontal axis indicates the number of H^- ions per unit cell [H^-], calibrated from the results of NMR experiments. Four H^- ions per unit cell ([H^-]=4) corresponds to the full incorporation of H^- ions. Because the total charge of caged anions is fixed at 2.3×10^{21} q cm^{-3}, we assume that O^{2-} ions act as a counter species to H^- ions and its concentration has a reverse dependence to that of H^- ions. The vertical axis on the right hand side indicates the number of electrons per unit cell [e^-]. The photogenerated electron concentration has a maximum at around half the maximum concentration of H^- ions ([H^-]= ~2), and after

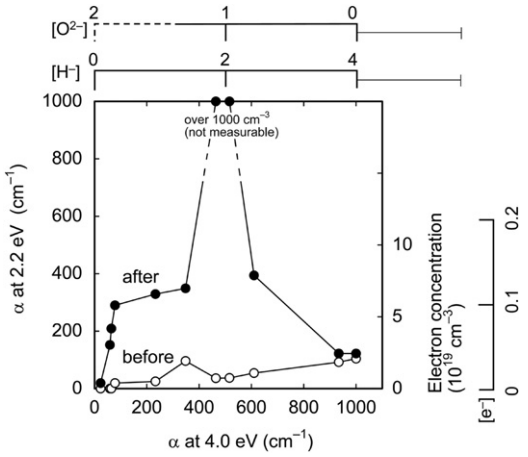

Fig. 4. Electron concentration before and after UV irradiation plotted as a function of H^- ion concentration. The H^- ion and electron concentrations were determined from absorption coefficients at the absorption edge (4.0 eV) and tails (2.2 eV) of the F^+ and polaron bands, respectively. The thin lines on the upper scales indicate the possible errors at [H^-]=4 and [O^{2-}]=0, where the brackets indicates the number of species per unit cell.

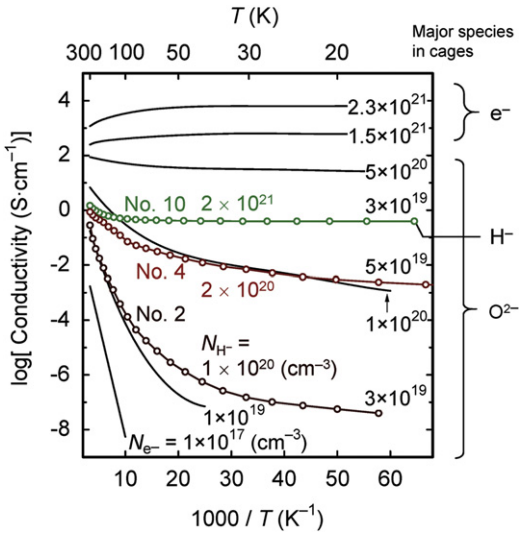

Fig. 5. Temperature–conductivity characteristics of samples 2, 4, and 10 (dark brown, brown, and green circles with lines). Data for electron-doped C12A7 samples reported in Refs. [27,28] (black solid lines) are plotted alongside for comparison. N_{e^-} (black) and N_{H^-} (dark brown, brown, and green) indicate the concentration of electrons and H^- ions, respectively. Electron concentrations were reevaluated according to the assessment in Ref. [32] (for interpretation of the references to color in this figure legend, the reader is referred to the web version of this article).

that, decreases with decreasing O^{2-} ion concentration. This dependence clearly indicates that generation of electrons by UV irradiation at room temperature requires the presence of both H^- and O^{2-} ions, validating the reaction shown in Eq. (5).

Conductivity–temperature characteristics of samples 2, 4, and 10 after UV irradiation are shown in Fig. 5 together with previously reported data concerning electron-doped C12A7 [27,28]. In the electron-doped samples, the electrical conductivity changes systematically from thermally activated hopping to metallic conductivity as the carrier electron concentration increases. In the lightly H^- ion-doped samples (2 and 4), the absolute electrical conductivity around room temperature and at low temperature characteristics are nearly the same as those in an electron-doped sample with a similar electron concentration. In contrast, sample 10, which is doped with nearly the theoretical maximum of H^- ions, does not exhibit the systematic dependence on electron concentration observed for the electron-doped samples. Despite its electron concentration being in the typical range for thermally activated hopping, its low temperature–conductivity shows little dependence on temperature similarly to the metallic ones. The difference in the conductivity characteristics are most likely ascribed to the differences in the dominant anion species in the cages: O^{2-} ions in the electron-doped samples exhibiting hopping conductivity and H^- ions in sample 10.

4. Discussion

4.1. Effect of H^- ion doping with high concentration

A red shift of the F^+ band with the increase of H^- ion concentration is found in Fig. 2. As a consequence, the color of the sample changes from green to olive. A similar shift has been observed in a series of electron-doped C12A7 samples with electron concentration higher than 1×10^{21} cm^{-3}. The origin of this red shift is ascribed to the release of lattice distortion caused by O^{2-} ions in cages [28,31]. Because the distribution of O^{2-} ions is random, some empty cages possess deeper potential wells for electron trapping than others. The occupation of electrons is more stable at deeper sites. Substitution of electrons or monovalent H^- ions for divalent O^{2-} ions may reduce the lattice distortion because of their weaker attraction for coordinating to Ca^{2+} ions in cages, averaging the electron trapping potentials in empty cages. As a result, the potential wells in the highly electron- or H^- ion-doped lattices become shallower compared with those in a lattice doped predominantly with O^{2-} ions. This effect decreases the F^+ transition energy, leading to the red shift of the relevant absorption band. Furthermore, the metallic-like conductivity of the heavily H^- ion-doped sample supports the idea of the release of the lattice distortion, because the averaged potential well of cages enhances inter-cage tunneling of electrons at low temperature.

4.2. Photogeneration of persistent electrons

As indicated in the upper scale in Fig. 4, we have assumed that main extraframework counter species to H^- ions are O^{2-} ions. According to a thermodynamic assessment in a previous study [33], if OH^- ions coexist with electrons, the thermal equilibration converts them to H^- and O^{2-} ions according to Eq. (5). Thus, the concentration of OH^- ions before UV irradiation is relatively small, particularly in samples containing a larger concentration of residual electrons in the as-prepared state. The enhancement of electron photogeneration in the H^- ion concentration range below [H^-]=2 is ascribed to the increase in the H^- ion concentration and the suppression above [H^-]=2 is ascribed to the decrease in the concentration of O^{2-} ions. These O^{2-} ions act as a

sink for H^+ ions converted from the H^- ions by releasing totally two electrons. The H^0 species in cage and OH^- group formed in the lattice framework, if any, are unstable transient states and are easily changes their chemical states to the extraframework H^- or OH^- ions. According to Eq. (5), the theoretical maximum number of photogenerated electrons per unit cell is determined by the smaller value of either $2[H^-]$ or $2[O^{2-}]$. The observed concentration of photogenerated electrons is in general limited to $\sim 1/10-1/100$ of the theoretical maximum. Probably, only extra-framework H^- and O^{2-} ions that are in an appropriate environment can complete the two-electron generation process. Because this process involves H^+ ion diffusion [14,37], the two ions need to be located in neighboring cages. The statistical probability for this may limit the generation of persistent electrons.

5. Conclusions

H^- ions can be incorporated in cages of C12A7 at concentrations up to the theoretical maximum ($[H^-]=\sim 4$) using a CaH_2 reduction process. The concentration of electrons that can be photogenerated in these H^- ion-doped C12A7 samples increases with increasing H^- ion concentration below $[H^-]=2$ and decreases above $[H^-]=2$. This indicates that O^{2-} ions are involved in the electron photogeneration process, validating the proposed reaction: $H^-(c)+O^{2-}(c)+null(c)\rightarrow 2e^-(c)+OH^-(c)$. Increased H^- ion doping intensifies the photoionization band with an absorption tail located at ~ 4.0 eV, and causes a red shift of the F^+ band (~ 2.8 eV). The latter is correlated with the release of lattice distortion and the metallic-like electrical conductivity of heavily H^- ion-doped C12A7.

Acknowledgment

This work was supported by a Grant-in-Aid for Elements Science and Technology (no. 08055013), and a Grant-in-Aid for Young Researchers A (no. 19685019) from the Ministry of Education, Culture, Sports, Science, and Technology of Japan.

References

[1] R.W. Pohl, Proc. Phys. Soc. 49 (1937) 3–31.
[2] G. Schaefer, J. Phys. Chem. Solids 12 (1960) 233–244.
[3] Y. Chen, M. Orera, R. Gonzalez, R.T. Williams, G.P. Williams, G.H. Rosenblatt, G.J. Pogatshnik, Phys. Rev. B 42 (1990) 1410–1416.
[4] R. Gonzalez, M.A. Monge, J.E. Munoz-Santiuste, R. Pareja, Y. Chen, E. Kotomin, M.M. Kukla, A.I. Popov, Phys. Rev. B (1999) 4786–4790.
[5] B. Malaman, J.F. Brice, J. Solid State Chem. 53 (1984) 44.
[6] S. Steinsvik, Y. Larring, T. Norby, Solid State Ionics 143 (2001) 103–106.
[7] F.W. Poulsen, Solid State Ionics 145 (2001) 387–397.
[8] M. Zumdick, G. Althoff, C. Röhr, Acta Crystallogr. C57 (2001) 339–340.
[9] M.A. Hayward, E.J. Cussen, J.B. Claridge, M. Bieringer, M.J. Rosseinsky, C.J. Kiely, S.J. Blundell, I.M. Marshall, F.L. Pratt, Sicence (2002) 1882–1884.
[10] A. Bowman, J.B. Claridge, M.J. Rosseinsky, Chem. Mater. (2006) 3046–3056.
[11] K. Hayashi, S. Matsuishi, T. Kamiya, M. Hirano, H. Hosono, Nature (2002) 462–465.
[12] M.I. Bertoni, T.O. Mason, J.E. Medvedeva, A.J. Freeman, K.R. Poeppelmeier, J. Appl. Phys. 97 (2005) 103713.
[13] S. Matsuishi, K. Hayashi, M. Hirano, H. Hosono, J. Am. Chem. Soc. 127 (2005) 12454–12455.
[14] K. Hayashi, P.V. Sushko, A.L. Shulger, M. Hirano, H. Hosono, J. Phys. Chem. B 109 (2005) 23836–23842.
[15] Ç. Kiliç, A. Zunger, Appl. Phys. Lett. 81 (2002) 73–75.
[16] C.G. Van de Walle, J. Neugebauer, Nature 423 (2003) 626–628.
[17] S.F.J. Cox, J. Phys. Condens. Matter 15 (2003) R1727–R1780.
[18] K. Hayashi, M. Hirano, H. Hosono, J. Phys. Chem. B 109 (2005) 11900–11906.
[19] D.K. Lee, L. Kogel, S.G. Ebbinghaus, I. Valov, H.D. Wiemhoefer, M. Lerch, J. Janek, Phys. Chem. Chem. Phys. 11 (2009) 3105–3114.
[20] R. Strandbakke, C. Kongshaug, R. Haugsrud, T. Norby, J. Phys. Chem. C 113 (2009) 8938–8944.
[21] T. Nomura, K. Hayashi, Y. Kubota, T. Kamiya, M. Hirano, M. Takata, H. Hosono, Chem. Lett. 36 (2007) 902–903.
[22] J. Jeevaratnam, F.P. Glasser, L.S.D. Glasser, J. Am. Ceram. Soc. 47 (1964) 105–106.
[23] K. Hayashi, P.V. Sushko, D. Munõz Ramo, A.L. Shluger, S. Watauchi, I. Tanaka, S. Matsuishi, M. Hirano, H. Hosono, J. Phys. Chem. B 111 (2007) 1946–1956.
[24] K. Hayashi, M. Hirano, S. Matsuishi, H. Hosono, J. Am. Chem. Soc. 124 (2002) 738–739.
[25] K. Hayashi, S. Matsuishi, N. Ueda, M. Hirano, H. Hosono, Chem. Mater. 15 (2003) 1851–1854.
[26] G.I. Zhmoidin, A.K. Chatterjee, Cem. Concr. Res. 14 (1984) 386–396.
[27] S. Matsuishi, Y. Toda, M. Miyakawa, K. Hayashi, T. Kamiya, M. Hirano, I. Tanaka, H. Hosono, Science 301 (2003) 626–629.
[28] S.W. Kim, S. Matsuishi, T. Nomura, Y. Kubota, M. Takata, K. Hayashi, T. Kamiya, M. Hirano, H. Hosono, Nano Lett. 7 (2007) 1138–1143.
[29] Y. Toda, H. Yanagi, E. Ikenaga, J.J. Kim, M. Kobata, S. Ueda, T. Kamiya, M. Hirano, K. Kobayashi, H. Hosono, Adv. Mater. 19 (2007) 3564–3569.
[30] L. Palacios, A. Cabeza, S. Bruque, S. Gracía-Granda, M.A.G. Aranda, Inorg. Chem. 47 (2008) 2661–2667.
[31] L. Palacios, S. Bruque, M.A.G. Aranda, Phys. Status Solidi B245 (2008) 666–672.
[32] T. Yoshizumi, S. Matsuishi, S.W. Kim, H. Hosono, K. Hayashi, J. Phys. Chem. C 114 (2010) 1534–1537.
[33] K. Hayashi, M. Hirano, H. Hosono, Bull. Chem. Soc. Jpn. 80 (2007) 872–884.
[34] P.V. Sushko, A.L. Shluger, K. Hayashi, M. Hirano, H. Hosono, Phys. Rev. Lett. 91 (2003) 126401.
[35] P.V. Sushko, A.L. Shluger, K. Hayashi, M. Hirano, H. Hosono, Thin Solid Films 445 (2003) 161–167.
[36] P.V. Sushko, A.L. Shluger, K. Hayashi, M. Hirano, H. Hosono, Appl. Phys. Lett. 86 (2005) 092101.
[37] P.V. Sushko, A.L. Shluger, K. Hayashi, M. Hirano, H. Hosono, Phys. Rev. B 73 (2006) 45120.
[38] Y. Tsujimoto, C. Tassel, N. Hayashi, T. Watanabe, H. Kageyama, K. Yoshimura, M. Takano, M. Ceretti, C. Ritter, W. Paulus, Nature 450 (2007) 1062–1066.
[39] S. Inoue, M. Kawai, N. Ichikawa, H. Kageyama, W. Paulus, Y. Shimakawa, Nat. Chem. 2 (2010) 213–217.